

Thermal shock behavior of tungsten based alloys manufactured via powder injection molding



ELSEVIER

Contents lists available at SciVerse ScienceDirect

Journal of Nuclear Materials

journal homepage: www.elsevier.com/locate/jnucmat



Thermal shock behavior of tungsten based alloys manufactured via powder injection molding



G. Pintsuk a,*, D. Blagoeva b, J. Opschoor c

- ^a Forschungszentrum Jülich, EURATOM-Association, D-52425 Jülich, Germany
- ^b Nuclear Research and Consultancy Group, P.O. Box 25, 1755 ZG Petten, The Netherlands
- ^c ECN, Energy research Centre of the Netherlands, P.O. Box 1, 1755 ZG Petten, The Netherlands

ARTICLE INFO

Article history: Available online 27 February 2013

ABSTRACT

The focus of this work is to address mechanical strength and recrystallization resistance through thermal shock investigation of newly developed fine grained tungsten base materials (i.e., pure tungsten and two doped tungsten-grades incorporating either 1 or 5 vol% Y_2O_3 produced via powder injection molding (PIM)). Therefore, repetitive ELM (edge localized mode)-like loads (n = 100) were applied by means of an electron beam at various temperatures between RT and 400 °C (673 K) with a pulse duration of 1 ms and an absorbed power density of up to 1.13 GW/m². The microstructural properties, e.g. grain size, and Y_2O_3 -particle distribution, were correlated with crack formation at a certain temperature, the crack propagation direction towards the bulk material and the amount of plastic deformation/surface roughening at higher temperatures. Thereby, it was shown that W–1 vol% Y_2O_3 outperformed all other investigated grades and reference materials from literature.

© 2013 Elsevier B.V. All rights reserved.

1. Introduction

A challenging issue for the development of a commercial fusion reactor will be choosing a suitable plasma-facing material. High demands, particularly in regards to long-life stability, will be placed on the chosen material. Factors that contribute to these demands include thermal loads, either applied in steady state or transient mode, combined He and hydrogen attack, and the impact of high energy neutrons causing material degradation and transmutation. The most promising materials yet seem to be tungsten or tungsten based materials. Despite good thermo-physical properties, low sputter threshold, and the comparably low neutron activation, the thermo-mechanical properties of these materials are less than ideal. Various R&D initiatives are in place to address the drawbacks of brittleness at low temperatures and increasing ductile to brittle transition temperature (DBTT) when irradiated with neutrons, after recrystallization, and by hydrogen inventory.

One initiative deals with the development of fine grained doped and undoped tungsten based materials manufactured via powder injection molding (PIM) [1]. Due to the near net-shape technology and high manufacturing temperatures, this method offers cost effective production and high resistance against grain growth and related mechanical degradation. The doped materials (e.g. commercially available tungsten grades containing La_2O_3) are oxide dispersion strengthened and contain different volume per-

centages of Y_2O_3 , which should have a positive effect on the material's strength, ductility, and workability and improve the recrystallization resistance. Y_2O_3 exhibits, in comparison to La₂O₃, a higher melting and boiling point ($\Delta T \approx 100$ K), which is important when dealing with thermal shock loads in the GW/m² range.

For the investigation of the performance of these materials under ELM-like loading conditions, thermal shock analyses were performed using an electron beam. Thereby, repetitive ELM like loads were applied at various temperatures and absorbed energy densities. By correlating the microstructural properties (i.e., grain size, Y_2O_3 -particle size and distribution) with the existence or non-existence of thermal-shock-induced and base-temperature-dependent crack formation, the materials behavior is qualified and subsequently compared to literature data [2–7] and an extensively characterized reference material [8,9].

2. Material and testing procedure

The investigated materials were produced by the Energieonderzoek Centrum Nederland (ECN), using PIM. The PIM method is a near net-shape process for the manufacturing of high-volume, high-precision components aiming primarily at producing relatively small and complex-shaped parts in small and large industrial quantities. The main features of materials produced according to this manufacturing route are high density, isotropy and microstructural stability at high temperatures. The latter is based on the one hand on sintering at temperatures >2000 °C

^{*} Corresponding author. Tel.: +49 2461 616383; fax: +49 2461 616435. *E-mail address*: g.pintsuk@fz-juelich.de (G. Pintsuk).

(>2273 K) and on the other hand can be influenced by fine dispersion of oxide or carbide particles.

The three newly developed PIM materials using very fine powders of <2 µm grain size are pure tungsten and two oxide dispersion strengthened (ODS) tungsten-alloys with 1 and 5 vol%Y2O3 (i.e., about 0.26 and 1.36 wt%, respectively). Thereby, pure tungsten was produced as a reference material to serve as basis for comparison with the other materials and evaluate the effect of the alloying elements (i.e., Y₂O₃). Small discs with a diameter of 9.6-9.75 mm and a height of 2.8 mm were produced to comply with the needs of thermal-shock testing. The investigation of the materials microstructure (Fig. 1) via metallography, etching (creating also some artifacts as the black dots inside single tungsten-grains), and image analysis shows a continuing decrease of the grain size with increasing content of Y_2O_3 down to a median area of 7.3 μ m² for W-5 vol 8 Y₂O₃. The generally round Y₂O₃-particles are thereby in the range from ${\sim}100\,\text{nm}$ up to $2\,\mu\text{m}$ (Fig. 2) acting as obstacles for grain growth. The particles are homogeneously distributed and located mainly at the large angle grain boundaries because mixing but not mechanical alloying has taken place.

The materials were characterized at Forschungszentrum Juelich by measuring the density by the Archimedes method, performing hardness measurements via Vickers indentation (HV1), and mea-

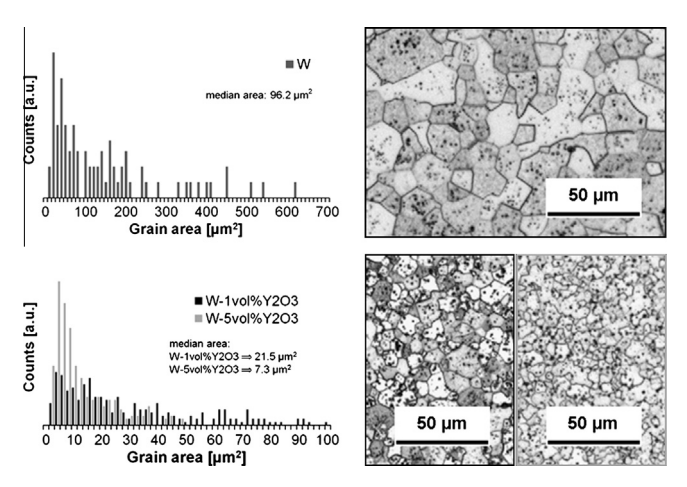


Fig. 1. Grain size distribution and median area size for pure tungsten, W-1 vol 3 Y₂O₃ and W-5 vol 3 Y₂O₃.

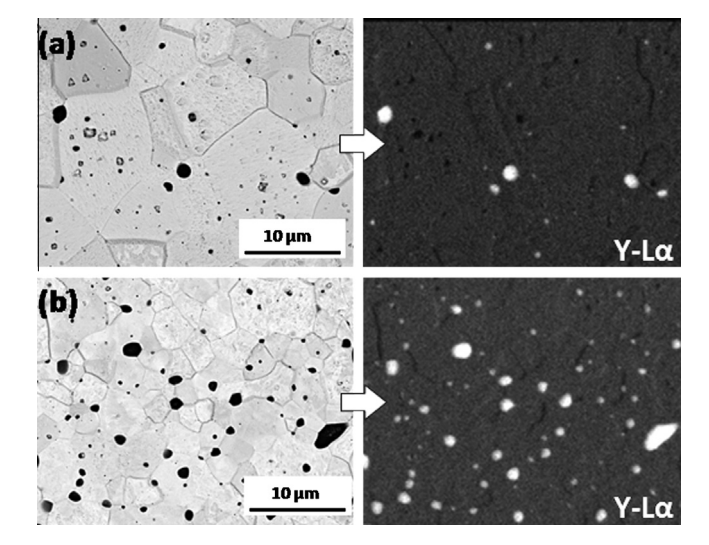


Fig. 2. SEM-micrographs and elemental mappings of (a) W-1 wt% Y_2O_3 and (b) W-5 wt% Y_2O_3 .

suring the thermal diffusivity as a function of temperature from room temperature (RT) to 1200 °C (1473 K) using a THETA laser flash apparatus. Further mechanical characterizations necessary for the understanding of the materials response to thermal shock loads were performed by Blagoeva et al. [10].

Finally, thermal shock experiments were performed in the electron beam facility JUDITH I, which provides an electron beam with a diameter at full width half maximum of 1 mm. Since the loaded area was 4×4 mm² the beam had to be scanned across the surface with frequencies in the x- and y-directions of 31 and 40 kHz, respectively, to obtain a homogeneously loaded surface. Despite the defect-free outer surface of the produced discs, the loaded front side of the samples was polished to ensure the comparability of the thermal shock tests, in particular, the quantification of surface roughness due to plastic deformation.

The experimental parameters simulating ELM-relevant conditions comprise the exposure to multiple shots (100/1000) at absorbed power densities of 0.19-1.13 GW/m² for 1 ms. The used absorption coefficient for tungsten was 0.55, which was determined by Monte-Carlo simulations. It was confirmed by absorbed current measurements that took also electrons into account that cause the emissions of low energy secondary electrons. The base temperature of the specimens was varied from RT to 400 °C (673 K) in order to obtain the thresholds for brittle crack formation [8]. During testing the specimens were monitored using an infrared camera. Related to the infrared images and depending on the individual thermal contact between specimen and holder, the testing frequency was adjusted between 0.1 and 0.3 Hz to guarantee a stable base temperature. Finally, post-mortem examinations were performed by laser profilometry and microscopic and metallographic means.

3. Results and discussion

Fig. 3 shows the materials density, which decreases with increasing Y_2O_3 content and was determined to lie between 94.6% of the theoretical value for W–5 vol% Y_2O_3 and 96% for pure tungsten. At the same time, the measured Vickers hardness HV1 significantly increases from pure tungsten to W–5 vol% Y_2O_3 by about 26% (Fig. 3). This indicates an increase in mechanical strength but also brittleness, which was confirmed by Blagoeva et al. [10]. Blagoeva et al. determined that the mechanical strength of the materials measured by bending tests and the ductile to brittle transition temperature (DBTT) measured via Charpy impact testing increased with Y_2O_3 content.

Besides these large differences in mechanical properties, only minor changes of the thermo-physical properties were found. The thermal diffusivity of all three materials is in a narrow range with W–1 vol% Y_2O_3 providing about 3–6% higher values than the other two (Fig. 4). The reason for this slight increase is unclear and cannot be explained by the microstructural findings. However, these results are about 5–20% lower than for an industrially manufactured tungsten grades with ultra-high purity [11], which results for the PIM produced tungsten grades in steeper thermal gradients during thermal-shocks and higher surface temperatures during steady-state heat loading.

Two main characteristics were determined from the thermal shock tests (Fig. 5), i.e., the power density related damage threshold, below which no detectable material and surface modification takes place, and the temperature related cracking threshold, determining the base temperature below which brittle crack formation takes place. Thereby, the damage threshold for all three materials was determined to be identical and between 0.19 and 0.38 GW/ m². In contrast, the cracking threshold varied significantly between the three materials. Despite some statistically triggered and

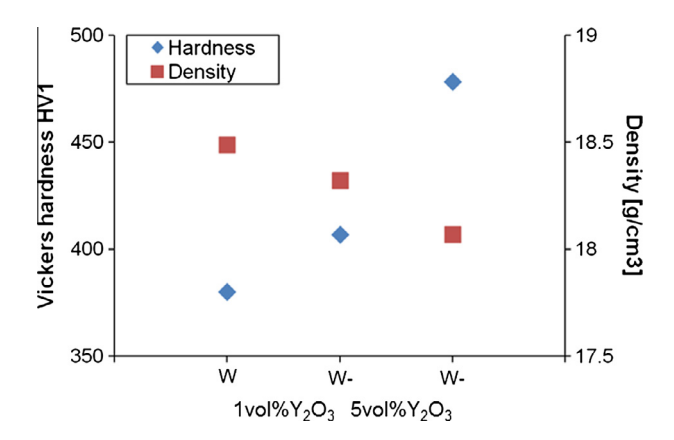


Fig. 3. Vickers hardness and density of pure tungsten, W–1 vol% Y_2O_3 and W–5 vol% Y_2O_3 .

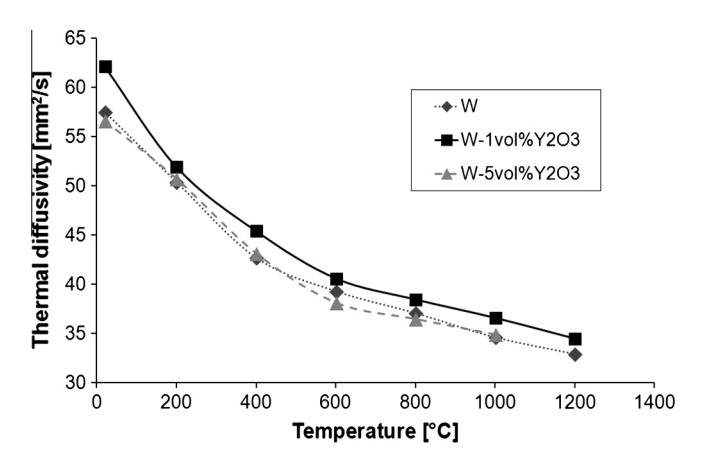


Fig. 4. Thermal diffusivity of pure tungsten, W–1 vol% Y_2O_3 and W–5 vol% Y_2O_3 as a function of temperature.

pulse-number related irregularities for pure tungsten (see test results at $100\,^{\circ}\text{C}/373\,\text{K}$) that have to be addressed carefully in future experiments, the threshold for pure tungsten and W–5 vol%Y $_2O_3$ is in the temperature range between $200\text{--}400\,^{\circ}\text{C}$ (473–673 K). At lower temperatures, brittle cracking resulted in crack formation along grain boundaries perpendicular and parallel to the loaded surface and in loosening of single grains in the cracked volume (Fig. 6a and c). The crack depth increased with increasing power density from $300\text{--}400\,\mu\text{m}$ to $850\text{--}1500\,\mu\text{m}$ at $0.38\,\text{GW/m}^2$ and $1.13\,\text{GW/m}^2$, respectively. In particular, the crack depth of up to $1500\,\mu\text{m}$ is significantly larger than the heat penetration depth of about $350\,\mu\text{m}$ for the 1 ms pulse [5,12] and therefore a clear proof for the materials brittleness.

In contrast, no cracking threshold but only strong surface roughening could be determined for W–1 vol% Y_2O_3 even when applying 1000 pulses at the most severe applied conditions, i.e., $1.13~\rm GW/m^2$ at RT (Fig. 6b). This is outstanding performance for this material grade in comparison to reference material grades [6,8] and comparable to expensive, high-end materials still in the developmental stage [13]. However, it contradicts mechanical test results, which showed that the DBTT increases due to the addition of Y_2O_3 . The reason for this behavior is still unknown but is expected to be related to the microstructural features of the material (e.g., the combination of grain size and particle distribution).

For comparison of the materials and the power- and temperature-dependent trends, the surface roughness, or more precisely the surface corrugation due to plastic deformation and crack for-

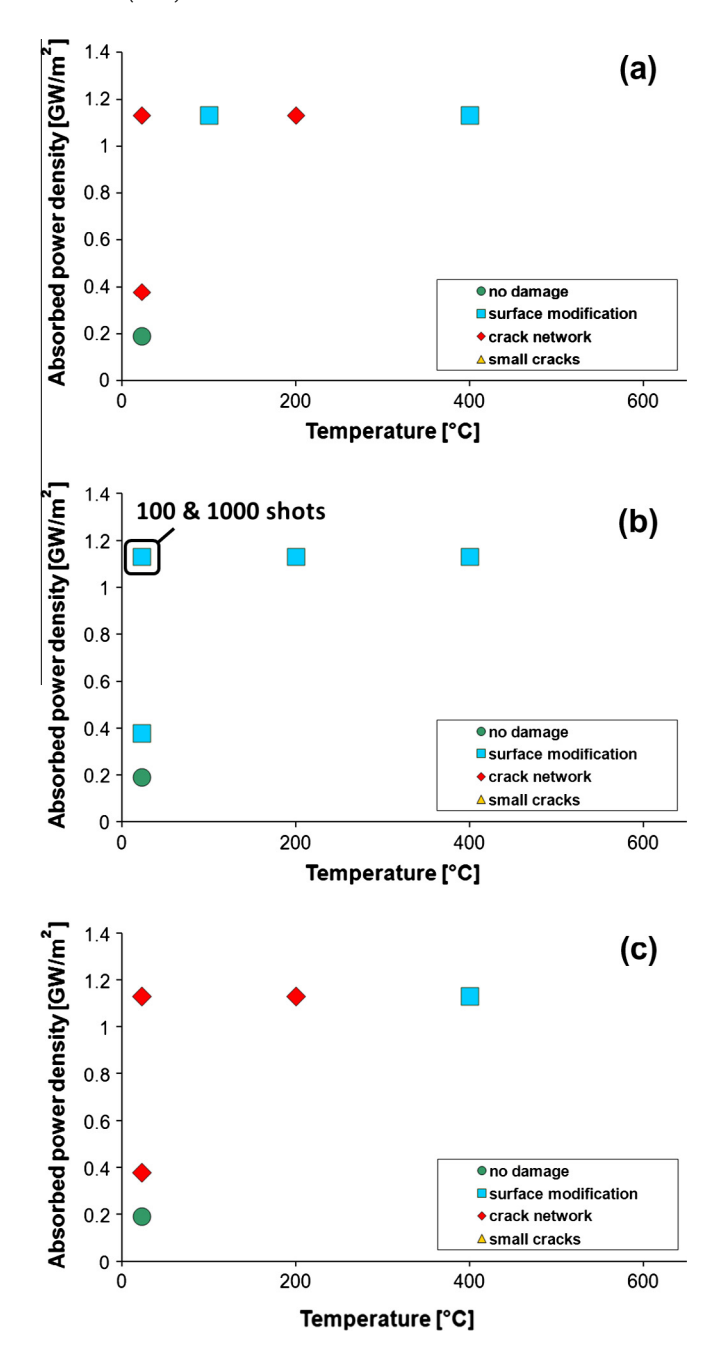


Fig. 5. Damage characteristics for (a) pure tungsten, (b) W–1 vol% Y_2O_3 and (c) W–5 vol% Y_2O_3 as a function of temperature and power density.

mation, was determined. The wave length for the determination of the R_a -value was set to 8 mm in x- and y-orientation so that the deformation and the cracking-induced waviness would be included in the results (Fig. 7). The original surface roughness after polishing is between 0.07 and 0.1 μ m, which corresponds to the values obtained after loading with 0.19 GW/m². At higher power densities R_a increases and W–1 vol%Y₂O₃ exhibits the lowest deformation values among all investigated materials due to the lack of crack formation, while W–5 vol%Y₂O₃ determines the upper limit (Fig. 7a). After applying 1000 pulses at RT and 1.13 GW/m² on W–1 vol%Y₂O₃, the surface roughness increases by almost a factor of 3. However, no crack formation was observed (Fig. 7b) indicating high tolerance against plastic strain. Subsequently, this might also benefit the thermal fatigue behavior of the material which was found to create cracks after a defined number of pulses as soon

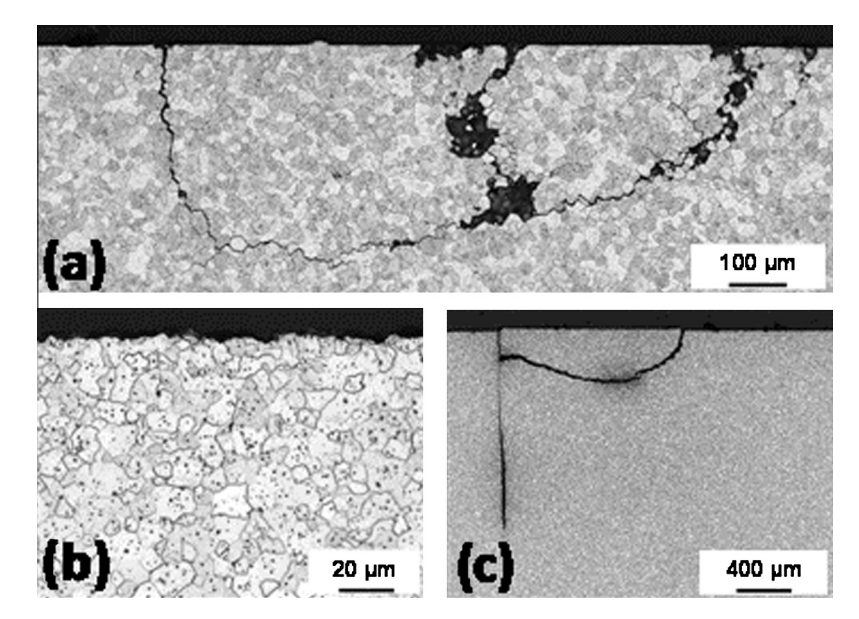


Fig. 6. Crack formation and surface roughening for (a) pure tungsten at 0.38 GW/m^2 at RT; (b) W-1 vol%Y₂O₃ at 1.13 GW/m^2 at RT and 1000 shots; (c) W-5 vol%Y₂O₃ at 1.13 GW/m^2 at RT.

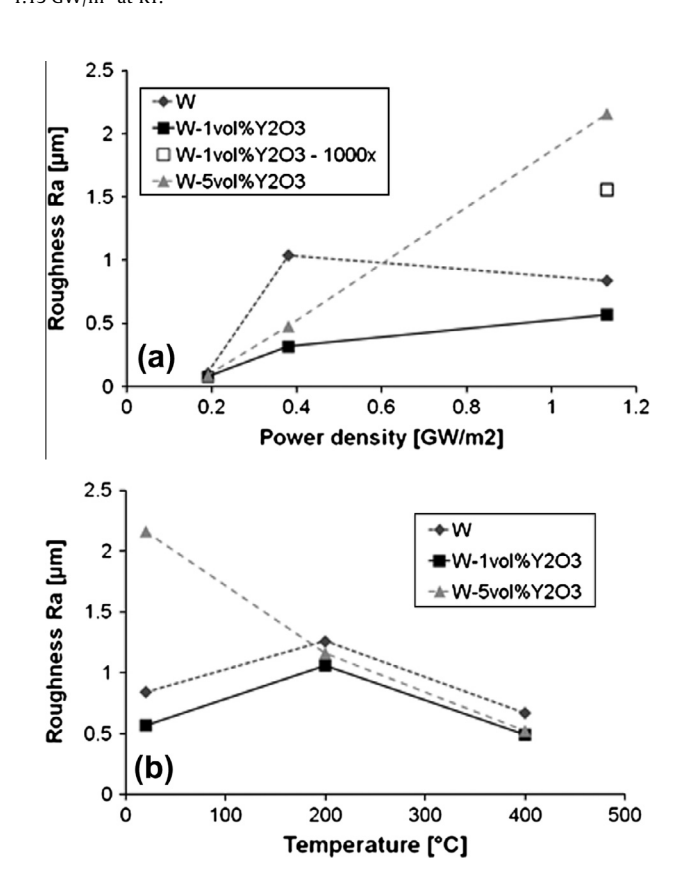


Fig. 7. Surface roughness as a function of (a) power density at RT and (b) temperature at a constant power density of 1.13 GW/m² (bottom).

as roughening occurs [9]. At temperatures $\geqslant\!200\,^{\circ}\text{C}$ (473 K) the roughness becomes almost identical for all three tungsten-grades (Fig. 7b). Thereby, the decrease from 200 °C to 400 °C (473 to 673 K) is related to the decreasing mechanical strength of the material with increasing temperature and therefore reduced compression forces from the bulk material on the loaded surface/volume and the increased plastic deformation of the bulk material itself.

4. Conclusion

Three different tungsten-grades (i.e., pure tungsten, W–1 vol 3 Y $_{2}$ O $_{3}$ and W–5 vol 3 Y $_{2}$ O $_{3}$ manufactured via PIM) were investigated as potential plasma facing materials with respect to microstructure, thermo-physical properties, hardness, and thermal shock response when exposed to ELM-like heat loads. The materials are characterized by an isotropic and fine grain size that decreases with increasing homogeneously distributed Y $_{2}$ O $_{3}$ content. Furthermore, the determined thermal diffusivity is about 10–20% lower than for industrially manufactured pure tungsten and exhibits no relevant variations while the mechanical properties strongly deviate among the three materials. This indicates an increase in hardness and mechanical strength with increasing content of Y $_{2}$ O $_{3}$.

The determination of cracking thresholds related to the individual DBTT, and power density related damage thresholds, revealed a superior behavior of W–1 vol%Y $_2$ O $_3$. No cracks were formed, only strong surface roughening up to 1000 shots at RT and 1.13 GW/ m 2 . For the other materials the cracking threshold was observed to be at temperatures >200 °C (473 K). Crack formation occurs perpendicular and parallel to the loaded surface and reaches a depth up to several times the heat penetration depth during thermal shock loading. The discrepancy between the three materials and in particular the superiority of W–1 vol%Y $_2$ O $_3$ does not correlate with the results of the mechanical analyses and therefore needs more detailed investigation.

Acknowledgements

This work, supported by the European Communities was carried out within the framework of the European Fusion Development Agreement. The views and opinions expressed herein do not necessarily reflect those of the European Commission. Furthermore V. Gutzeit and E. Wessel are greatly acknowledged for their support with metallographic investigations and EDX-analyses.

References

- [1] Tungsten and Tungsten Alloy Development: Final, Report, NRG-22671/11.106179, January 2011.
- [2] A. Zhitlukhin, N. Klimov, I. Landman, J. Linke, A. Loarte, M. Merola, V. Podkovyrov, G. Federici, B. Bazylev, S. Pestchanyi, V. Safronov, T. Hirai, V.

- Maynashev, V. Levashov, A. Muzichenko, J. Nucl. Mat. 363-365 (2007) 301-
- [3] K. Wittlich et al., Fus. Eng. Des. 84 (2009) 1982-1986.
- [4] N. Klimov, V. Podkovyrov, A. Zhitlukhin, D. Kovalenko, J. Linke, G. Pintsuk, I. Landman, S. Pestchanyi, B. Bazylev, G. Janeschitz, A. Loarte, M. Merola, T. Hirai, G. Federici, B. Riccardi, I. Mazul, R. Giniyatulin, L. Khimchenko, V. Koidan, J. Nucl. Mat 415 (1) (2011) S59-S64.
- [5] Y. Ueda, M. Toda, M. Nishikawa, K. Kondo, K.A. Tanaka, Fus. Eng. Des. 82 (2007) 1904-1910.
- [6] T. Hirai, G. Pintsuk, J. Linke, M. Batilliot, J. Nucl. Mat. 390–391 (2009) 751–754. [7] G. Pintsuk, I. Uytdenhouwen, Int. J. Ref. Met. Hard Meter. 28 (6) (2010) 661–
- [8] G. Pintsuk, A. Prokhodtseva, I. Uytdenhouwen, J. Nucl. Mater. 417 (1-3) (2011) 481-486.
- 19 Th. Loewenhoff, A. Bürger, J. Linke, G. Pintsuk, A. Schmidt, L. Singheiser, C. Thomser, Phys. Scr. T145 (2011) 014057. 4pp.
- [10] D. Blagoeva, J. Opschoor, J.G. van der Laan, C. Sarbu, G. Pintsuk, M. Jong, T. Bakker, P. ten Pierick, H. Nolles, J. Nucl. Mater. 442 (2013) S198–S203.
- [11] M. Wirtz, J. Linke, G. Pintsuk, L. Singheiser, I. Uytdenhouwen, Phys. Scr. T145 (2011) 014058. 4pp.
- [12] T. Hirai, G. Pintsuk, Fus. Eng. Des. 82 (4) (2007) 389–393.
- [13] G. Pintsuk, H. Kurishita, J. Linke, H. Arakawa, S. Matsuo, T. Sakamot, S. Kobayashi, K. Nakai, Phys. Scr. T145 (2011) 014060. 5pp.

